NANO LETTERS

Letter

pubs.acs.org/NanoLett

Plasmonic Radiance: Probing Structure at the Ångström Scale with Visible Light

Benjamin Gallinet,[†] Thomas Siegfried,[‡] Hans Sigg,[‡] Peter Nordlander,[§] and Olivier J. F. Martin*[,†]

[†]Nanophotonics and Metrology Laboratory, Swiss Federal Institute of Technology (EPFL), CH-1015 Lausanne, Switzerland

[‡]Laboratory for Micro. and Nanotechnology, Paul Scherrer Institut, 5232 Villigen PSI, Switzerland

[§]Department of Physics and Astronomy, M.S. 61 Laboratory for Nanophotonics, Rice University, Houston, Texas 77251-1892, United States

S *Supporting Information*

ABSTRACT: Plasmonic modes with long radiative lifetimes combine strong nanoscale light confinement with a narrow spectral line width carrying the signature of Fano resonances, making them very promising for nanophotonic applications such as sensing, lasing, and switching. Their coupling to incident radiation, also known as radiance, determines their optical properties and optimal use in applications. In this work, we theoretically and experimentally demonstrate that the radiance of a plasmonic mode can be classified into three different regimes. In the weak coupling regime, the line shape exhibits remarkable sensitivity to the dielectric environment. We show that geometrical displacements and deformations at the Ångström scale can be detected optically by measuring the radiance. In the intermediate regime, the electromagnetic energy stored in the mode is maximal, with large electric field enhancements that can be exploited in surface enhanced spectroscopy applications. In the strong coupling regime, the interaction can result in hybridized modes with tunable energies.

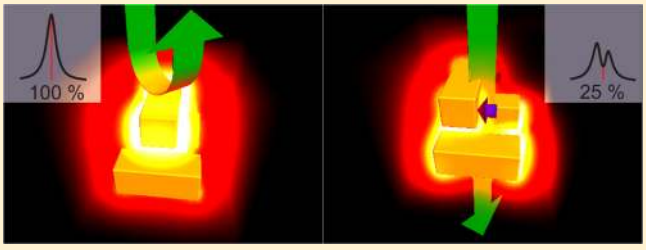

KEYWORDS: *Fano resonances, electromagnetically induced transparency, plasmonic nanosensors, surface enhanced Raman scattering (SERS), extraordinary optical transmission*

With their ability to concentrate light at a deep-subwavelength scale by excitation of surface plasmons, metallic nanostructures play a major role in current nanoscience.[1] In particular, optical tweezers,[2] antennas,[3,4] lasers,[5] photodetectors,[6] or biochemical sensing platforms[7,8] have been scaled down to the nanometer range. However, their performance are limited by the short lifetimes of surface plasmon resonances.[9] Recently, it has been shown that the use of plasmonic modes with long radiative life times (subradiant modes) can drastically enhance the performance of nanophotonic devices.[10−12] Their spectral response carry an asymmetric line shape with sharp spectral features, characteristic of Fano resonances.[13−22] The coupling of subradiant modes to radiation, their radiance, is directly controlled by the geometrical configuration of the nanostructures,[19] and also governs their optical response and the location and amplitude of light confinement.[20] Despite the fact that the use of subradiant modes for nanophotonic applications critically depends on the coupling strength, the choice of an optimal regime has so far never been addressed.

In this work, we use a universal model for interacting radiative and localized channels to investigate the radiance of a plasmonic mode. We demonstrate that the radiance of a plasmonic mode can be classified into three different regimes. In the weak coupling regime, the radiance of the mode is small and extremely sensitive to perturbations in the coupling. We introduce a novel sensing concept, radiance sensing, which is based on the sensitivity of the radiance to the environment, rather than conventional plasmon sensing relying on the wavelength shift of plasmon modes.[8] In the intermediate regime, the radiative damping is equal to the intrinsic damping, and the radiance does not depend strongly on the coupling. However for this critical coupling, the electromagnetic energy stored in the mode is maximal and associated to large electromagnetic field enhancements. For strong coupling, the optical response can result in two distinct and broad hybridized modes.[23] We illustrate these universal findings theoretically and experimentally on two very different plasmonic nanostructures. Specifically, we study a plasmonic nanostructure consisting of a dipolar nanorod antenna on top of two parallel nanorods supporting a nonradiative quadrupolar mode. The other specific example consists of subwavelength slits in a metallic film fabricated with extreme ultraviolet interference lithography (EUV−IL). In this system, the plasmon mode supported by the individual nanowires serves as the subradiant mode, and its radiance is controlled by changing the width of the gap. The facile tuning of the coupling in this nanostructure makes it

Received: October 23, 2012
Revised: December 19, 2012
Published: December 28, 2012

ACS Publications © 2012 American Chemical Society

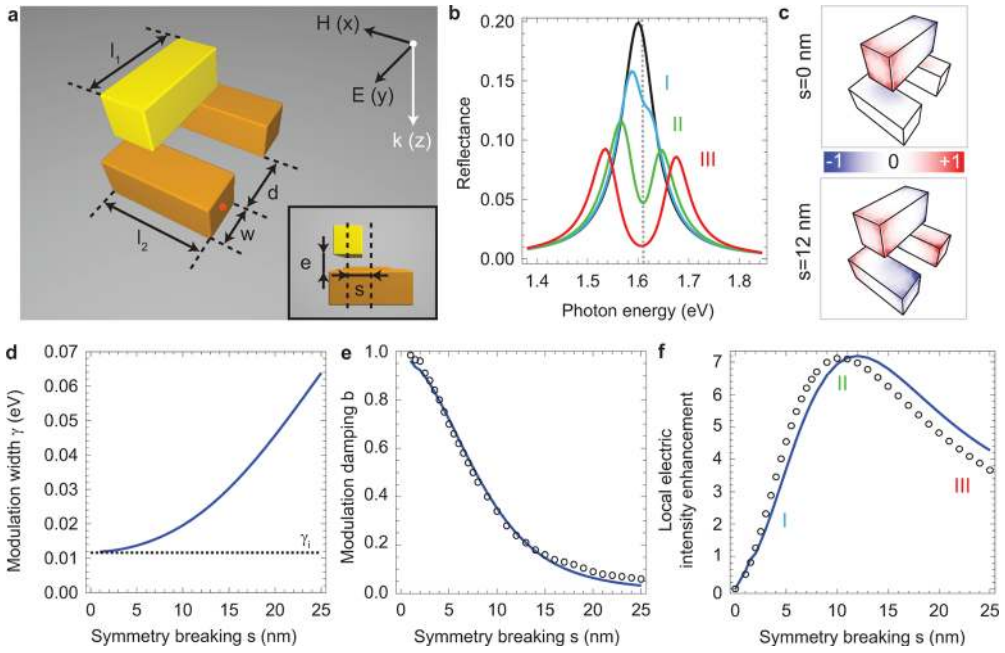

Figure 1. Symmetry breaking in a plasmonic nanostructure. (a) Schematic of a single nanostructure and definition of the geometrical parameters: $l_1 = l_2 = 100$ nm, $w = 40$ nm, $d = 60$ nm, $e = 20$ nm. (b) Reflectance of a two-dimensional array with period 500 nm in both x and y directions for various values of the symmetry breaking s. The permittivity of gold is interpolated from experimental data,[24] and the refractive index of the surrounding environment is 1.33 (water). The black, blue, red, and green curves correspond to $s = 0$ nm, $s = 5$ nm, $s = 12$ nm, and $s = 25$ nm, respectively. In the system with broken symmetry, the resonant excitation of the quadrupolar mode supported by the bottom nanoparticles induces a modulation of the reflectance spectrum. The symbols I, II, and III represent the three different coupling regimes. (c) Surface charge distribution at a resonant energy 1.61 eV for $s = 0$ nm and $s = 12$ nm, respectively. (d) Spectral width of the modulation as a function of the symmetry breaking. The solid blue and the dashed black lines represent the total and the intrinsic width, respectively. (e) Modulation damping b as a function of the symmetry breaking. The solid blue line corresponds to the ratio of the reflectance at a photon energy of 1.61 eV in the symmetry broken system ($s \neq 0$) to the reflectance in the symmetric system ($s = 0$) at the same energy. The black circles correspond to calculations using panel d and the expression of b in eq 2. In panels d and e, the modulation width and damping are fitted from eq 1 for $q = 0$. (f) Electric field intensity enhancement related to the quadrupolar mode at 1.61 eV as a function of the symmetry breaking. The solid blue line corresponds to a direct evaluation at 4 nm from the surface of the bottom bar, as shown by a red point in panel a. The black circles correspond to calculations using panel d and eq 3.

possible to reach all three levels of radiance. In the weak coupling regime, we show that radiance sensing enables the detection of gap widths at the sub-nanometer scale. Using surface-enhanced Raman scattering (SERS), we verify that the largest electric field enhancement occurs in the intermediate regime.

Figure 1a illustrates the geometry of a plasmonic nanostructure characterized by a Fano-resonant response.[25] Each unit cell consists of a metallic nanoparticle placed on top of two parallel metallic nanoparticles. The top nanoparticle supports a plasmonic mode with a dipolar distribution of charges and acts as an antenna for receiving and emitting light. The two bottom nanoparticles support a hybridized plasmonic mode with a quadrupolar distribution of charges. In the quasistatic approximation, the out-of-phase dipole moments of the quadrupolar mode forbids far−field radiation. In the symmetric configuration ($s = 0$), only the antenna mode can be excited by the homogeneous field of a plane wave. The spectra of the nanostructure array are calculated with a full-field numerical method based on the solution of surface integrals.[26,27] As shown in the reflectance spectrum of Figure 1b, the antenna resonance appears as a Lorentzian centered around $\omega_a = 1.599$ eV with a spectral width of $\gamma_a = 0.040$ eV. A relative displacement s of the top antenna from the symmetric position allows the coupling of light into the quadrupolar mode resulting in an antiresonance (dip) of the reflectance (see Figure 1c). The resonance width γ of the quadrupolar mode is given by the sum of two contributions: the intrinsic damping γ_i and the radiative contribution γ_c. For simplicity, in the following we will refer to the coupling between these two modes as γ_c although strictly speaking the radiative damping will depend both on the coupling and antenna properties. The intrinsic width γ_i is associated with nonradiative decay by the Joule effect in the metallic nanostructures and corresponds to the minimal value of the total spectral width γ. As the mode coupling is increased by symmetry breaking (increasing s, as shown in Figure 1d), the quadrupolar mode broadens, and the contribution of γ_c to the spectral width increases.

In the symmetry-broken configuration, the light impinging onto the system can follow two pathways: it is either directly scattered by the antenna or re-emitted after indirect excitation of the quadrupolar mode. The destructive interference between the direct and the indirect pathways yields a window of transparency, as a plasmonic equivalent to electromagnetically induced transparency.[14,25] In the more general case where the antenna mode is detuned from the quadrupolar mode, both destructive and constructive interference can be observed. The resulting reflectance profile is modulated by an asymmetric line shape characteristic of Fano resonances.[16,21,28,29] Around the resonance frequency of the quadrupolar mode ω_0, the reflectance spectrum R is the product of the antenna reflectance R_a by the asymmetric modulation function:[19,29]

dx.doi.org/10.1021/nl303896d | Nano Lett. 2013, 13, 497−503

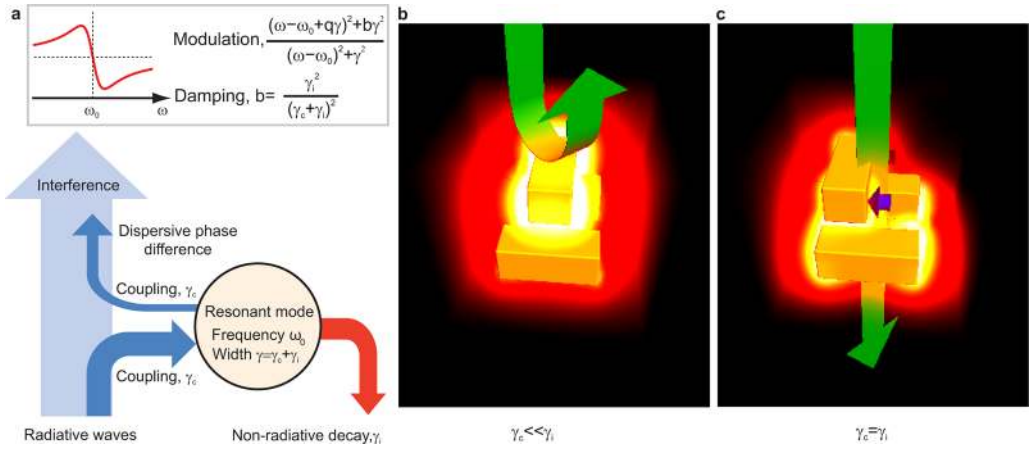

Figure 2. Fano interference and radiance sensors. (a) A mode of resonance frequency ω_o is weakly coupled to a continuum of radiative waves with constant γ_c. The in-coupled energy is either lost by nonradiative decay with constant γ_i or recoupled to the continuum. The total resonance spectral width is $\gamma = \gamma_c + \gamma_i$. Due to destructive or constructive interference between the direct and the indirect pathways, the spectral response is modulated by an asymmetric line shape. The parameter q, known as the Fano parameter, describes the degree of asymmetry. Nonradiative decay prevent full interference, resulting in a modulation damping. The modulation damping parameter b is given by the ratio of the intrinsic width to the total width. (b) For low radiative coupling $\gamma_c \ll \gamma_i$, the resonant mode is weakly excited, corresponding to full reflectance in the plasmonic nanostructure. (c) For balanced lifetimes $\gamma_c = \gamma_i$, the resonant mode is fully excited, and transparency is observed. Only a nanometer-scale geometrical perturbation is necessary for this switching process, which can be used for the design of ultrasensitive nanosensors.

$$R = R_a \frac{(\omega - \omega_0 + q\gamma)^2 + b\gamma^2}{(\omega - \omega_0)^2 + \gamma^2} \quad (1)$$

where q and b describe the modulation asymmetry and modulation damping, respectively. In the case where the mode detuning is small compared to the antenna resonance width γ_a, the modulation is symmetric ($q = 0$), and the modulation damping b becomes the ratio of the reflectance at the minimum of the anti-resonance in the symmetry-broken configuration ($s \neq 0$) to the reference reflectance in the symmetric configuration ($s = 0$) at the same frequency: $R(\omega_0) = R_a(\omega_0)b$. As the mode coupling is increased, the modulation becomes more pronounced (see Figure 1e): the modulation damping ranges from 1 in the weak coupling regime ($\gamma_c \ll \gamma_i$) and decreases monotonically to 0 in the strong coupling regime ($\gamma_c \gg \gamma_i$). For weak coupling, the modulation amplitude is extremely sensitive to the symmetry breaking. A relative displacement of 12 nm of the antenna induces 75% variation of reflectance. However, the monotonic behavior of the modulation parameters in the far-field reflectance spectra does not appear in the near-field. In Figure 1f, the electric field intensity enhancement associated with the quadrupolar mode initially increases along with the modes coupling but reaches a maximum for a specific value of the mode coupling and then decreases. The same behavior is reproduced for an isolated structure (see Figure S1 in the Supporting Information).

The local near-field intensity enhancement depends on the total energy stored by the mode and the modal field distribution. As will be shown in the next subsection, the energy flow through a subradiant mode is the key parameter determining its radiance and role in Fano interference. Thus the results in Figure 1f allows us to classify the radiance of a subradiant mode into three distinct regimes: a weak coupling regime (I) where the mode energy increases monotonically with coupling; an intermediate regime (II) where the mode energy is maximal and the radiance is only weakly dependent on coupling; a strong coupling regime (III) where the mode excitation decreases with increasing coupling. The identification of energy transfer as the key parameter determining the radiance of the subradiant mode provides crucial insight for the rational design of Fano-resonant structures for specific applications. For instance, in sensing applications, the system should be positioned in the weak coupling regime. As will be demonstrated below, the extreme sensitivity to geometrical perturbations is due to a reversal of the relative role of the radiative and nonradiative contributions to the total damping. In SERS applications, the system should be in the intermediate coupling regime where the electromagnetic energy stored in the subradiant mode is maximal.

To provide more insights into the interplay between radiative and nonradiative decay, we introduce a general model for coupling of radiative and localized channels (see Figure 2). The trade-off between radiative and nonradiative decays is a fundamental issue in quantum optics, in particular for the control of spontaneous emission,[30−32] and we will explicitly investigate it in Fano-resonant systems. The localized channel is a spectrally narrow resonant mode, such as the quadrupolar mode in Figure 1. This mode is coupled to a continuum of radiative waves with constant γ_c (the role of the dipole antenna is only to enhance the coupling efficiency between the resonant mode and the continuum). The in-coupled energy is either lost by nonradiative decay with a damping rate γ_i or by reciprocity recoupled to the continuum with a rate γ_c. Due to the constructive and destructive interference between the continuum and the recoupled wave, the amplitude of the observed signal carries an asymmetric signature. The nonradiative and radiative lifetimes of the resonant mode are given by γ_i^{-1} and γ_c^{-1}, respectively. During this process of energy exchange between the continuum and the resonant mode, part of the light intensity is decayed nonradiatively, which prevents complete destructive and constructive interference. The portion of light intensity which does not contribute to the interference is the modulation damping and is given by the ratio of the intrinsic width to the total width (eq S38 in the Supporting Information):

dx.doi.org/10.1021/nl303896d | Nano Lett. 2013, 13, 497−503

$$b = \frac{\gamma_i^2}{(\gamma_c + \gamma_i)^2} \quad (2)$$

Let us now consider the electromagnetic energy storage in the resonant mode. In a conservative system ($\gamma_i = 0$) more energy would be stored in the mode with decreasing coupling. In a nonideal case, however, intrinsic losses introduce dissipation, so that energy accumulation in the mode is negligible for very weak coupling. In the weak coupling regime (I), the modulation depth rapidly evolves as the radiative channel opens up for the resonant mode. As the coupling increases, the in-coupled energy balances the intrinsic losses, and the energy storage in the mode reaches a maximum (coupling regime II). For stronger coupling (III), the radiative channel limits the energy stored in the mode which decreases. The electromagnetic energy stored in the resonant mode has the following behavior as a function of the coupling:

$$\text{stored energy} \propto \frac{\gamma_c}{(\gamma_c + \gamma_i)^2} \quad (3)$$

derived in the Supporting Information. The regime of high energy storage (II) occurs when the radiative and nonradiative losses exactly compensate each other ($\gamma_c = \gamma_i$), which is analogous to the impedance matching condition in the design of antennas.[10] This condition which we will refer to as the critical coupling, corresponds to $b = 1/4$ and can thus be deduced from the far-field pattern. The quantitative relations between modulation damping and energy storage drawn from this model are valid for any linear wave-propagating system with coupled radiative and nonradiative channels. In particular, the decomposition into three coupling regimes and the corresponding behavior of the modulation damping parameter are very well reproduced in the plasmonic nanostructure of Figure 1. The extreme sensitivity of the plasmonic nanostructure to geometrical perturbations in the weakly interacting regime (I) stems from a transfer from low to full excitation of the resonant mode. During the process, light switches from total reflectance (see Figure 2b) to transparency (see Figure 2c).

The model system sketched in Figure 3a consisting of two coupled oscillators A and B, introduced as a mechanical analogue of Fano resonances,[33] provides a particularly simple and intuitive corroboration of the mechanisms described in our two-channel model. The oscillator A is forced and has a high damping constant γ_a modeling both radiative and nonradiative losses of the antenna mode, whereas the oscillator B has a low damping constant γ_i associated only to nonradiative losses. The equivalents of eqs 1, 2, and 3 for this system can be derived and expressed directly in the harmonic oscillator parameters (see the Supporting Information), which shows the universality of our approach. In Figure 3b, the two oscillators have different resonance frequencies, and the modulation is asymmetric.[19] This more general case of destructive and constructive interference corresponds to $q \neq 0$ in eq 1. The presence of the resonant mode alters the intrinsic properties of the radiative channel, so that the spectral response is altered for strong coupling. In Figure 3c, the mode energy is equivalent to the amplitude of the oscillator B, which also increases as a function of the oscillator coupling and reaches a maximum when the coupling γ_c balances intrinsic losses γ_i. As the coupling increases, the width γ of the modulation becomes comparable to the width γ_a of the oscillator A. For strong coupling, a

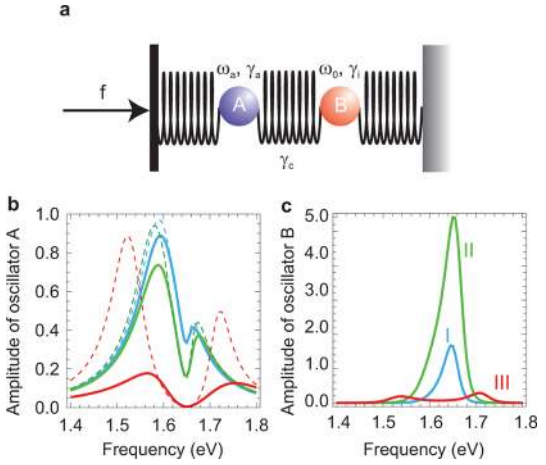

Figure 3. Mechanical analogue of Fano interference. (a) A forced oscillator A with frequency ω_a and large damping γ_a modeling a plasmon mode with both radiative and nonradiative losses, is coupled with constant γ_c to a free oscillator B with frequency ω_0 and low damping γ_i modeling a plasmon mode with nonradiative losses only. (b–c) Amplitude of the oscillators (b) A and (c) B as a function of the frequency, with $\hbar\omega_a = 1.599$ eV, $\hbar\gamma_a = 0.060$ eV, $\hbar\omega_0 = 1.650$ eV, and $\hbar\gamma_i = 0.012$ eV. The blue, green, and red curves correspond to $\hbar\gamma_c = 0.003$ eV, $\hbar\gamma_c = 0.009$ eV, and $\hbar\gamma_c = 0.082$ eV, respectively. The solid and dashed line correspond to the direct evaluation from the equations of motion and to the evaluation with eq 1, respectively.

splitting in the response of the oscillator B is observed, each individual resonance being a normal mode of the composite system, and the dip in the spectral response of oscillator A of the system is not Fano interference but just the sum of two Lorentzians centered on each hybridized mode.[23,34,35] This limiting case is the classical analogue of Autler–Townes splitting.[33,34,36]

As an experimental illustration of the model, the optical properties of plasmons in a sub-wavelength array of gold nanostructures were investigated as a function of the nearest-neighbor separation distance (see Figure 4). In this system, the radiative channel is given by the light directly transmitted through the slits. This forms a nonresonant radiative continuum, in contrast to what was the case for the nanostructure of Figure 1 where a resonant dipole antenna coupled to the radiative continuum acts as the immediate emitter–receptor. Here, the plasmon associated the individual wires plays the role of the resonant mode weakly coupled to radiation. Figure S2 of the Supporting Information shows that the plasmon mode is excited only for an electric field polarization perpendicular to the wires, and at the resonance frequency hot spots are observed at the edges of the nanowires. For very small slit openings, the plasmon mode is not efficiently excited, and the reflectance in Figure 4b is close to that of an infinite gold film. As the gap opens, the coupling of the plasmon mode to the radiative continuum increases. The destructive interference of light re-emitted by the plasmon mode with the directly reflected light results in a dip in the reflectance spectrum and enhanced transmission through the nanoslits.[37] With this interference process which is also the physical origin of extraordinary optical transmission,[1,37] less light is reflected than the ratio of metal filling the unit cell (see Figure 4c).

The opening of the gap increases the amount of light entering the slit and as a consequence the coupling of the

dx.doi.org/10.1021/nl303896d | Nano Lett. 2013, 13, 497–503

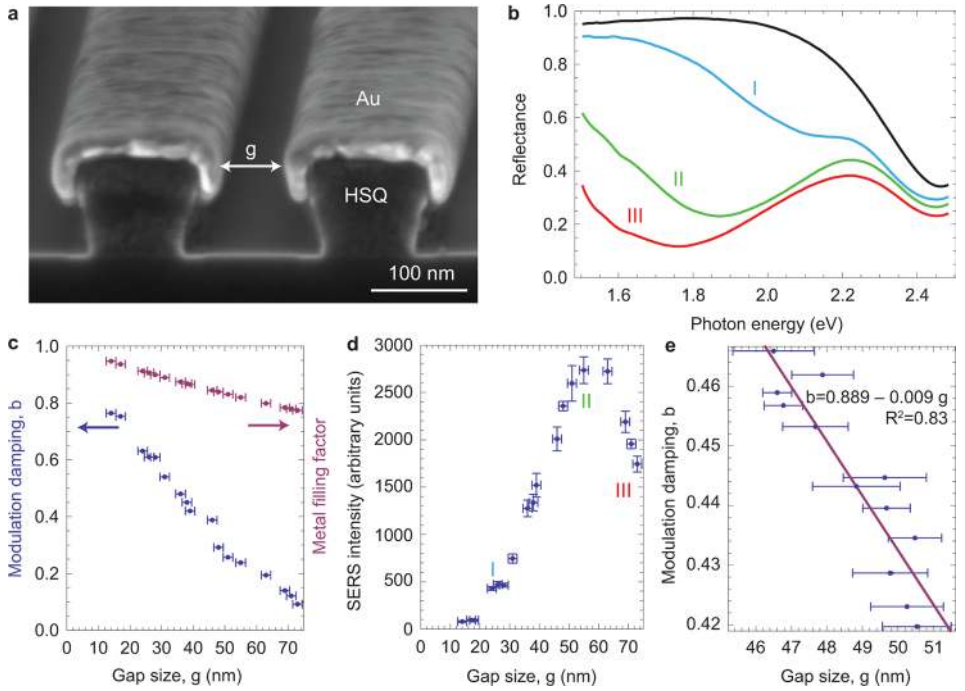

Figure 4. Control of slit opening in a sub-wavelength array of gold nanostructures. (a) Cross section scanning electron micrograph (SEM) of an array fabricated with extreme ultraviolet interference lithography and shadow evaporation. The underlying grating has a periodicity of 250 nm, a depth of 120 nm, and a spacing of 110 nm between two lines. The gold layer thickness is 38 nm. (b) Reflectance spectra for various values of the gap size. The black, blue, red, and green curves correspond to g = 0 nm, g = 36 nm, g = 61 nm, and g = 75 nm. A surface plasmon resonance is excited in the gap between two neighboring nanostructures. The interference of the gap plasmon with the directly reflected light yields a window of transmission. (c) Modulation damping as a function of the gap size g, compared to the metal filling factor defined as the ratio (period−gap)/period. (d) The surface enhanced Raman scattering (SERS) intensity of a benzeneethanethiol monolayer excited at 633 nm, proportional to the fourth power of the electric field enhancement, is measured as a function of the gap size g. (e) Optical spectra are collected stepwise along a 600 μm long pattern with a gold layer thickness of 45 nm. Multiple SEM images are recorded along the same axis of the optical measurements to compare the average gap size to the modulation damping. Horizontal error bars correspond to the standard deviation of the average gap size measured with SEM over the area of illumination.

plasmon mode to the radiative continuum. The ratio of the nonradiative to the radiative decay rate of the plasmon mode decreases and as a consequence also the modulation damping (see Figure 4c). To probe the corresponding variation in near-field intensity, we measure the SERS response of molecules adsorbed at the surface of the sample, enhanced as a function of the fourth power of the electric field amplitude.[8,38] In Figure 4d, the SERS signal from the array is measured as a function of the gap size. Similarly to the reflectance, the SERS signal strongly depends on the polarization.[39] A maximum is observed for a gap of 55 ± 1.5 nm, and the corresponding value of the modulation damping parameter is 0.24. This value is in very good agreement with our universal theoretical prediction of maximal energy storage for 1/4, confirming experimentally the validity of the existence of a critical coupling for optimal near-field enhancement. The modulation damping b is used here as direct quantitative indicator of the radiative decay rate. During the opening of the gap to full excitation of the plasmon mode (regime I), a change of 75% of the modulation damping is observed. In this regime, variations of the gap size measured with scanning electron microscopy (SEM) are probed optically by directly measuring the modulation damping: a linear fit of slope 0.009 nm^{-1} is obtained (see Figure 4e). The horizontal error bars correspond to the standard deviation of the gap size measured with SEM over the area of illumination, which can reach the sub-nanometer scale. In these cases, the distance from the average of the gap size to the trendline is comparable to the standard deviation. This implies that, by using the trendline as a calibration curve, a measurement of the gap size at the sub-nanometer scale can be performed. With this method, the measurement is not limited by the spectral resolution of the apparatus.

Surface plasmon modes are extremely sensitive to perturbations of their radiance. The new concept of radiance sensing uses this advantage when the optical response of a subradiant mode switches from a nonresonant to a fully resonant situation. We now compare this approach to standard localized surface plasmon sensing, where the perturbation is monitored via a spectral shift of the resonance.[7,8,12] For approaches where the shift is calculated by fitting the entire line shape to an analytical formula,[12,19,20] the accuracy and stability of the fit in detecting a perturbation depends on the strength of the intensity variations of the line shape. In experimental measurements, the accuracy is determined by the signal-to-noise ratio, which also depends on the strength of the intensity variation at a fixed frequency. We therefore consider the strength of the intensity variations for a given displacement as the sensitivity of the system. Considering the system of Figure 1, a perturbation is applied to the interparticle distance so that a spectral shift of the subradiant mode is observed (Figure S3 of the Supporting Information). The sensitivity with respect to the antenna position in Figure S1 (controlling the radiance of the subradiant mode) is more than five times larger than the sensitivity with respect to the interparticle distance in Figure S3. This shows that radiance sensing is able to surpass the performance of standard localized surface plasmon sensing. In

dx.doi.org/10.1021/nl303896d | Nano Lett. 2013, 13, 497−503

our particular experimentally fabricated gap array, radiance sensing has been used to detect geometrical displacements at the Ångström scale.

In conclusion, by analyzing the energy flow through a subradiant optical mode coupled to a radiative continuum, we have shown that the radiance of the subradiant mode is the key parameter determining its optical properties. We have demonstrated that the radiance can be classified as belonging to one of three different regimes: weak, intermediate, or strong interaction. This insight provides the key element of understanding needed for rational design of structures for optimal performance of a broad range of nano-optical devices such as nanoantennas,[3,4,10] plasmonic lasers,[40−42] infrared metamaterial,[12,43] optomechanical,[44] nonlinear devices,[45,46] and chemical and biological sensors.[8] For the weak radiance situation, we have introduced a novel concept of sensing, radiance sensing, and experimentally show that this sensing approach allows for detection of Ångström sized geometrical displacements. The development of ultra sensitive sensors based on radiance sensing has significant potential in a wide range of applications, such as in molecular rulers[11,47] for monitoring noninvasively chemical or biological processes, strain sensors,[48] for optical trapping and manipulation,[2,49] or in combination with specific materials for indirect sensing (for instance the pH,[50] the presence of hydrogen, or the local temperature[51]).

■ ASSOCIATED CONTENT

Supporting Information

Details of fabrication, optical and structural characterization, derivation of eqs 1, 2, and 3. This material is available free of charge via the Internet at http://pubs.acs.org.

■ AUTHOR INFORMATION

Corresponding Author

*E-mail: olivier.martin@epfl.ch.

Notes

The authors declare no competing financial interest.

■ ACKNOWLEDGMENTS

B.G. and O.J.F.M. acknowledge funding from CCMX−FanoSense. T.S. acknowledges funding from the Swiss Federal foundation. P.N. acknowledges funding from the Robert A. Welch Foundation (C-1222) and the Defense Threat Reduction Agency (HDTRA1-11-1-0040). B.G. would like to thank H. Giessen for stimulating discussions. T.S. would like to thank Y. Ekinci (PSI) and M. Vockenhuber (PSI) for their support. Part of this work was performed at the Swiss Light Source.

■ REFERENCES

(1) Genet, C.; Ebbesen, T. W. Light in tiny holes. *Nature* **2007**, *445*, 39−46.

(2) Juan, M. L.; Righini, M.; Quidant, R. Plasmon nano-optical tweezers. *Nat. Photonics* **2011**, *5*, 349−356.

(3) Muhlschlegel, P.; Eisler, H. J.; Martin, O. J. F.; Hecht, B.; Pohl, D. W. Resonant optical antennas. *Science* **2005**, *308*, 1607−1609.

(4) Novotny, L.; van Hulst, N. Antennas for light. *Nat. Photonics* **2011**, *5*, 83−90.

(5) Berini, P.; De Leon, I. Surface plasmon-polariton amplifiers and lasers. *Nat. Photonics* **2012**, *6*, 16−24.

(6) Knight, M. W.; Sobhani, H.; Nordlander, P.; Halas, N. J. Photodetection with Active Optical Antennas. *Science* **2011**, *332*, 702−704.

(7) Anker, J. N.; Hall, W. P.; Lyandres, O.; Shah, N. C.; Zhao, J.; Van Duyne, R. P. Biosensing with plasmonic nanosensors. *Nat. Mater.* **2008**, *7*, 442−453.

(8) Halas, N. J.; Lal, S.; Chang, W.-S.; Link, S.; Nordlander, P. Plasmons in Strongly Coupled Metallic Nanostructures. *Chem. Rev.* **2011**, *111*, 3913−3961.

(9) Brongersma, M. L.; Shalaev, V. M. Applied Physics The Case for Plasmonics. *Science* **2010**, *328*, 440−441.

(10) Seok, T. J.; Jamshidi, A.; Kim, M.; Dhuey, S.; Lakhani, A.; Choo, H.; Schuck, P. J.; Cabrini, S.; Schwartzberg, A. M.; Bokor, J.; Yablonovitch, E.; Wu, M. C. Radiation Engineering of Optical Antennas for Maximum Field Enhancement. *Nano Lett.* **2011**, *11*, 2606−2610.

(11) Liu, N.; Hentschel, M.; Weiss, T.; Alivisatos, A. P.; Giessen, H. Three-Dimensional Plasmon Rulers. *Science* **2011**, *332*, 1407−1410.

(12) Wu, C.; Khanikaev, A. B.; Adato, R.; Arju, N.; Yanik, A. A.; Altug, H.; Shvets, G. Fano-Resonant Asymmetric Metamaterials for Ultrasensitive Spectroscopy and Identification of Molecular Monolayers. *Nat. Mater.* **2012**, *11*, 69−75.

(13) Christ, A.; Martin, O. J. F.; Ekinci, Y.; Gippius, N. A.; Tikhodeev, S. G. Symmetry Breaking in a Plasmonic Metamaterial at Optical Wavelength. *Nano Lett.* **2008**, *8*, 2171−2175.

(14) Zhang, S.; Genov, D. A.; Wang, Y.; Liu, M.; Zhang, X. Plasmon-Induced Transparency in Metamaterials. *Phys. Rev. Lett.* **2008**, *101*, 047401.

(15) Verellen, N.; Sonnefraud, Y.; Sobhani, H.; Hao, F.; Moshchalkov, V. V.; Van Dorpe, P.; Nordlander, P.; Maier, S. A. Fano Resonances in Individual Coherent Plasmonic Nanocavities. *Nano Lett.* **2009**, *9*, 1663−1667.

(16) Ruan, Z.; Fan, S. Temporal Coupled Mode Theory for Fano Resonance in Light Scattering by a Single Obstacle. *J. Phys. Chem. C* **2010**, *114*, 7324−7329.

(17) Luk'yanchuk, B.; Zheludev, N. I.; Maier, S. A.; Halas, N. J.; Nordlander, P.; Giessen, H.; Chong, C. T. The Fano Resonance in Plasmonic Nanostructures and Metamaterials. *Nat. Mater.* **2010**, *9*, 707−715.

(18) Miroshnichenko, A. E.; Flach, S.; Kivshar, Y. S. Fano Resonances in Nanoscale Structures. *Rev. Mod. Phys.* **2010**, *82*, 2257−2298.

(19) Gallinet, B.; Martin, O. J. F. Influence of Electromagnetic Interactions on the Line Shape of Plasmonic Fano Resonances. *ACS Nano* **2011**, *5*, 8999−9008.

(20) Gallinet, B.; Martin, O. J. F. The Relation Between Near-field and Far-field Properties of Plasmonic Fano Resonances. *Opt. Express* **2011**, *19*, 22167−22175.

(21) Giannini, V.; Francescato, Y.; Amrania, H.; Phillips, C. C.; Maier, S. A. Fano Resonances in Nanoscale Plasmonic Systems: A Parameter-Free Modeling Approach. *Nano Lett.* **2011**, *11*, 2835−2840.

(22) Francescato, Y.; Giannini, V.; Maier, S. A. Plasmonic Systems Unveiled by Fano Resonances. *ACS Nano* **2012**, *6*, 1830−1838.

(23) Prodan, E.; Radloff, C.; Halas, N.; Nordlander, P. A Hybridization Model for the Plasmon Response of Complex Nanostructures. *Science* **2003**, *302*, 419−422.

(24) Johnson, P. B.; Christy, R. W. Optical-Constants of Noble-Metals. *Phys. Rev. B* **1972**, *6*, 4370.

(25) Liu, N.; Langguth, L.; Weiss, T.; Kaestel, J.; Fleischhauer, M.; Pfau, T.; Giessen, H. Plasmonic Analogue of Electromagnetically Induced Transparency at the Drude Damping Limit. *Nat. Mater.* **2009**, *8*, 758−762.

(26) Gallinet, B.; Martin, O. J. F. Scattering on Plasmonic Nanostructures Arrays Modeled with a Surface Integral Formulation. *Photonic Nanostruct.* **2010**, *8*, 278−284.

(27) Gallinet, B.; Kern, A. M.; Martin, O. J. F. Accurate and Versatile Modeling of Electromagnetic Scattering on Periodic Nanostructures with a Surface Integral Approach. *J. Opt. Soc. Am. A* **2010**, *27*, 2261−2271.

(28) Fano, U. Effects of Configuration Interaction on Intensities and Phase Shifts. *Phys. Rev.* **1961**, *124*, 1866.

(29) Gallinet, B.; Martin, O. J. F. Ab Initio Theory of Fano Resonances in Plasmonic Nanostructures and Metamaterials. *Phys. Rev. B* **2011**, *83*, 235427.
(30) Thomas, M.; Greffet, J. J.; Carminati, R.; Arias-Gonzalez, J. R. Single-molecule spontaneous emission close to absorbing nanostructures. *Appl. Phys. Lett.* **2004**, *85*, 3863−3865.
(31) Carminati, R.; Greffet, J. J.; Henkel, C.; Vigoureux, J. M. Radiative and non-radiative decay of a single molecule close to a metallic nanoparticle. *Opt. Commun.* **2006**, *261*, 368−375.
(32) Kern, A. M.; Meixner, A. J.; Martin, O. J. F. Molecule-Dependant Plasmonic Enhancement of Fluorescence and Raman Scattering near Realistic Nanostructures. *ACS Nano* **2012**, *6*, 9828−9836.
(33) Alzar, C. L. G.; Martinez, M. A. G.; Nussenzveig, P. Classical Analog of Electromagnetically Induced Transparency. *Am. J. Phys.* **2002**, *70*, 37−41.
(34) Anisimov, P. M.; Dowling, J. P.; Sanders, B. C. Objectively Discerning Autler-Townes Splitting from Electromagnetically Induced Transparency. *Phys. Rev. Lett.* **2011**, *107*, 163604.
(35) Liu, N.; Kaiser, S.; Giessen, H. Magnetoinductive and Electroinductive Coupling in Plasmonic Metamaterial Molecules. *Adv. Mater.* **2008**, *20*, 4521−4525.
(36) Autler, S. H.; Townes, C. H. Stark effect in rapidly varying fields. *Phys. Rev.* **1955**, *100*, 703−722.
(37) Pardo, F.; Bouchon, P.; Haidar, R.; Pelouard, J.-L. Light Funneling Mechanism Explained by Magnetoelectric Interference. *Phys. Rev. Lett.* **2011**, *107*, 093902.
(38) Ye, J.; Wen, F.; Sobhani, H.; Lassiter, J. B.; Dorpe, P. V.; Nordlander, P.; Halas, N. J. Plasmonic Nanoclusters: Near Field Properties of the Fano Resonance Interrogated with SERS. *Nano Lett.* **2012**, *12*, 1660−1667.
(39) Siegfried, T.; Ekinci, Y.; Solak, H. H.; Martin, O. J. F.; Sigg, H. Fabrication of sub-10 nm gap arrays over large areas for plasmonic sensors. *Appl. Phys. Lett.* **2011**, *99*, 263302.
(40) Bergman, D. J.; Stockman, M. I. Surface Plasmon Amplification by Stimulated Emission of Radiation: Quantum Generation of Coherent Surface Plasmons in Nanosystems. *Phys. Rev. Lett.* **2003**, *90*, 027402.
(41) Zheludev, N. I.; Prosvirnin, S. L.; Papasimakis, N.; Fedotov, V. A. Lasing Spaser. *Nat. Photonics* **2008**, *2*, 351−354.
(42) Ma, R.-M.; Oulton, R. F.; Sorger, V. J.; Bartal, G.; Zhang, X. Room-temperature sub-diffraction-limited plasmon laser by total internal reflection. *Nat. Mater.* **2011**, *10*, 110−113.
(43) Cubukcu, E.; Zhang, S.; Park, Y.-S.; Bartal, G.; Zhang, X. Split ring resonator sensors for infrared detection of single molecular monolayers. *Appl. Phys. Lett.* **2009**, *95*, 043113.
(44) Weis, S.; Riviere, R.; Deleglise, S.; Gavartin, E.; Arcizet, O.; Schliesser, A.; Kippenberg, T. J. Optomechanically Induced Transparency. *Science* **2010**, *330*, 1520−1523.
(45) Tuovinen, H.; Kauranen, M.; Jefimovs, K.; Vahimaa, P.; Vallius, T.; Turunen, J.; Tkachenko, N. V.; Lemmetyinen, H. Linear and second-order nonlinear optical properties of arrays of noncentrosymmetric gold nanoparticles. *J. Nonlinear Opt. Phys. Mater.* **2002**, *11*, 421−432.
(46) Zhang, Y.; Grady, N. K.; Ayala-Orozco, C.; Halas, N. J. Three-Dimensional Nanostructures as Highly Efficient Generators of Second Harmonic Light. *Nano Lett.* **2011**, *11*, 5519−5523.
(47) Sonnichsen, C.; Reinhard, B. M.; Liphardt, J.; Alivisatos, A. P. A molecular ruler based on plasmon coupling of single gold and silver nanoparticles. *Nat. Biotechnol.* **2005**, *23*, 741−745.
(48) Pryce, I. M.; Aydin, K.; Kelaita, Y. A.; Briggs, R. M.; Atwater, H. A. Highly Strained Compliant Optical Metamaterials with Large Frequency Tunability. *Nano Lett.* **2010**, *10*, 4222−4227.
(49) Zhang, W.; Huang, L.; Santschi, C.; Martin, O. J. F. Trapping and Sensing 10 nm Metal Nanoparticles Using Plasmonic Dipole Antennas. *Nano Lett.* **2010**, *10*, 1006−1011.
(50) Nunes, S. P.; Behzad, A. R.; Hooghan, B.; Sougrat, R.; Karunakaran, M.; Pradeep, N.; Vainio, U.; Peinemann, K.-V. Switchable pH-Responsive Polymeric Membranes Prepared via Block Copolymer Micelle Assembly. *ACS Nano* **2011**, *5*, 3516−3522.
(51) Langhammer, C.; Larsson, E. M.; Kasemo, B.; Zoric, I. Indirect Nanoplasmonic Sensing: Ultrasensitive Experimental Platform for Nanomaterials Science and Optical Nanocalorimetry. *Nano Lett.* **2010**, *10*, 3529−3538.